Carbohydrate Polymers 83 (2011) 1263–1273

Contents lists available at ScienceDirect

Carbohydrate Polymers

journal homepage: www.elsevier.com/locate/carbpol

A water-soluble methylated *N*-(4-*N*,*N*-dimethylaminocinnamyl) chitosan chloride as novel mucoadhesive polymeric nanocomplex platform for sustained-release drug delivery

Maleenart Petchsangsai[a], Warayuth Sajomsang[a], Pattarapond Gonil[a], Onanong Nuchuchua[a], Boonsong Sutapun[b], Satit Puttipipatkhachorn[c], Uracha Rungsardthong Ruktanonchai[a,*]

[a] *National Nanotechnology Center, National Science and Technology Development Agency, 111 Thailand Science Park, Pathumthani 12120, Thailand*
[b] *Photonics Technology Laboratory, National Electronics and Computer Technology Center, National Science and Technology Development Agency, 111 Thailand Science Park, Pathumthani 12120, Thailand*
[c] *Department of Manufacturing Pharmacy, Faculty of Pharmacy, Mahidol University, Bangkok 10400, Thailand*

ARTICLE INFO

Article history:
Received 2 June 2010
Received in revised form
19 September 2010
Accepted 20 September 2010
Available online 24 September 2010

Keywords:
Diclofenac sodium
Mucoadhesive
Nanocomplex
Quaternary chitosan derivative
Sustained release

ABSTRACT

A water-soluble chitosan derivative, methylated *N*-(4-*N*,*N*-dimethylaminocinnamyl) chitosan chloride (MDMCMChC) was investigated as novel mucoadhesive polymeric nanocomplex platform for sustained-release drug delivery in comparison with widely used chitosan derivative, *N*,*N*,*N*-trimethylammonium chitosan chloride (TMChC). Diclofenac sodium (DS) was used as model negatively charged drug in this study. The presence of *N*-(4-*N*,*N*,*N*-trimethylammoniumylcinnamyl) moieties in MDMCMChC resulted in very small (approximately 90 nm) and uniform in size of nanocomplexes, high drug entrapment and sustained release. Ionic interaction between both positively charged chitosan derivatives and DS was confirmed by FT-IR spectroscopy, however, the salt effect study suggested that electrostatic interaction plays an important role on nanocomplex formation of TMChC than MDMCMCh. The nanocomplex formation between MDMCMChC and DS is expected to be initially driven by electrostatic attraction between these two ionic species and later by hydrophobic interaction between the aromatic moiety of MDMCMChC and the aromatic ring of DS, resulting in enhanced molecular association and stabilized nanocomplexes. Moreover, the mucoadhesive property of DS/MDMCMChC nanocomplexes was comparable to TMChC confirmed by surface plasmon response (SPR) method. The obtained results, therefore, revealed high potential of methylated *N*-(4-*N*,*N*-dimethylaminocinnamyl) chitosan chloride as novel mucoadhesive polymeric nanocomplex platform for sustained-release drug delivery.

1. Introduction

Chitosan, a linear polysaccharide obtained by deacetylation of a naturally occurring polymer chitin, consists of β-(1,4)-2-amino-2-deoxy-D-glucopyranose units (GlcN) and a small amount of 2-acetamido-2-deoxy-D-glucopyranose or *N*-acetyl-D-glucosamine (GlcNAc) residues. Due to its non-toxicity, biodegradability and biocompatibility, Chitosan has been extensively reported on its potential use for both pharmaceutical and medical applications (Illum, 1998; Prabaharan & Mano, 2005). Additionally, mucoadhesive properties of chitosan have been reported, which can possibly due to its positive charges to interact with negative charges of mucus membrane (Nagarwal, Kant, Singh, Maiti, & Pandit, 2009). However, chitosan has shown some limitations because of its poor water solubility. To solve this problem, many chemical modifications of chitosan have been synthesized. *N*,*N*,*N*-Trimethylammonium chitosan chloride (TMChC) (Fig. 1a) has been proposed as one of water-soluble chitosan derivatives over a wide pH range (Domard, Rinaudo, & Terrassin, 1986; Domard, Gey, Rinaudo, & Terrassin, 1987; Muzzarelli & Tanfani, 1985; Sandri et al., 2005). Moreover, the effectiveness of TMChC against an array of common bacteria (gram-positive as well as gram-negative) and fungi (Jia, Shen, & Xu, 2001; Rúnarsson et al., 2007; Sajomsang, Gonil, & Saesoo, 2009) has been reported. Apart from that, TMChC has been widely studied and proposed as another mean of biomaterials according to its mucoadhesive properties (Sajomsang, Ruktanonchai, Gonil, & Nuchuchua, 2009; Van der Lubben, Verhoef, Borchard, & Junginger, 2001; Van der Merwe, Verhoef, Verheijden, Kotzé, & Junginger, 2004) and penetration enhancement (Chen et al., 2008; He, Guo, & Zhang, 2008; Jintapattanakit, Mao, Kissel, & Junyaprasert, 2008; Sandri et al., 2005).

In this study, a water-soluble chitosan derivative, methylated *N*-(4-*N*,*N*-dimethylaminocinnamyl) chitosan chloride (MDMCMChC), which has been previously synthesized and reported by

* Corresponding author. Tel.: +66 02564 7100x6552; fax: +66 02564 6981.
E-mail address: uracha@nanotec.or.th (U.R. Ruktanonchai).

0144-8617/$ – see front matter © 2010 Elsevier Ltd. All rights reserved.
doi:10.1016/j.carbpol.2010.09.033

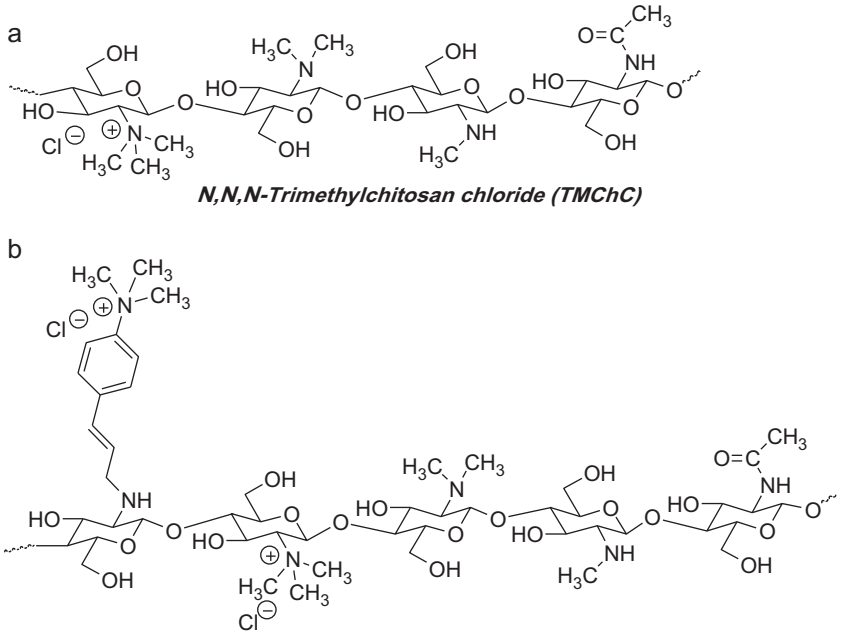

Fig. 1. Chemical structure of chitosan derivatives: *N*,*N*,*N*-trimethyl chitosan chloride, TMChC (a) and methylated *N*-(4-*N*,*N*,*N*-trimethylcinnamyl) chitosan chloride DMCMChC (b).

our group on its antibacterial activity (Sajomsang, Gonil, et al., 2009), mucoadhesive property and biocompatibility (Sajomsang, Ruktanonchai, et al., 2009), were evaluated in terms of its interaction with negatively charged drug and physicochemical properties of the obtained nanocomplexes compared with TMChC (Fig. 1). Diclofenac sodium (DS), a non-steroidal anti-inflammatory drug (NSAID), normally taken to reduce eye inflammation, treating pain, redness and swelling, was chosen as model negative charged drug. Since DS has strong negative charges, it can therefore spontaneously from nanocomplexes with positively charged chitosan. The chitosan derivative was substituted with dimethylaminocinnamyl moieties to improved binding ability with the drug and it was then quaternized to render chitosan soluble. A number of variables that influence the binding efficiency such as weight ratio of drug/polymer and chemical structure were investigated and compared with TMChC as a control on particle size, zeta potential, entrapment efficiency, mucoadhesive property and drug release.

2. Materials and methods

2.1. Materials

Chitosan was purchased from Seafresh Chitosan (Lab) Co., Ltd (Bangkok, Thailand). The degree of deacetylation of chitosan was determined to be 94% by ^{1}H NMR spectroscopy. A dialysis tubing with M_w cut-off of 12,000–14,000 g/mol from Cellu Sep T4, Membrane Filtration Products, Inc. (Segiun, TX, USA) was used to purify chitosan derivatives and study *in vitro* drug release. 4-Dimethylaminocinnamaldehyde, acetate buffer and Tris base were purchased from Fluka (Deisenhofen, Germany). Sodium cyanoborohydride, iodomethane, and 1-methyl-2-pyrrolidone were purchased from Acros Organics (Geel, Belgium). Carboxymethyldextran hydrogel (CMD500) sensor chips (25.0 diameter × 1.0 mm thickness) were purchased from Xantec bioanalytics (Duesseldorf, Germany). N-Hydroxysuccinimide (NHS), ethanolamine HCl and 1-ethyl-3-(3-dimethylaminopropyl) carbodiimide hydrochloride (EDC), diclofenac sodium (DS), ss-mucin type III powder and polyacrylic acid (~140 kDa) were purchased from Sigma–Aldrich, Inc. (USA). Sodium chloride, potassium chloride, sodium phosphate dibasic anhydrous, and potassium phosphate monobasic were purchased from Merck (Darmstadt, Germany). Sodium iodide was purchased from Carlo Erba Reagent (Rodano, Italy). The water used for all experiments was purified water obtained from a MilliQ Plus (Millipore, Schwalbach, Germany). All other reagents used were commercially available and were of analytical grade.

2.2. Synthesis of N-(4-N,N-dimethylaminocinnamyl) chitosan derivative

N-(4-*N*,*N*-Dimethylaminocinnamyl) chitosan (DMCMCh) was synthesized in accordance with a previously reported procedure (Chen et al., 2008; Sajomsang, Gonil, et al., 2009). In brief, chitosan (2.0 g, 12.22 mmol) was dissolved in 1% (v/v) of acetic acid (150 mL). The solution was diluted with ethanol (100 mL) and 4-dimethylaminocinnamaldehyde (1.0 mequiv./GlcN, 2.1 g) was added and stirred at room temperature for 12 h. The pH of the solution was adjusted to 5 with 15% (w/v) of sodium hydroxide. Subsequently, sodium cyanoborohydride (3.08 g, 48.92 mmol) was added and stirred at room temperature for 24 h, followed by pH adjustment to 7 with 15% (w/v) of sodium hydroxide. The reaction mixture was then dialyzed in distilled water and freeze-dried (2.95 g, 77.6% yield).

DMCMCh. FT-IR; ν 3427 (O–H and N–H, GlcN), 2919, 2866, and 2799 (C–H, GlcN), 1659 (N–H, GlcNAc), 1611 and 1518 (C=C, Aromatic), 1148 (C–O–C, GlcN), 1064 and 1028 cm^{-1} (C–O, GlcN), 804 cm^{-1} (C–H, Aromatic). ^{1}H NMR (CD_3COOD): δ 7.4 (m, 4H, Ph), 4.8 (s, 1H, H-1), 4.5 (d, 2H, $C\underline{H}_2$-NH), 4.5-3.3 (m, 5H, H3-H6) 3.1 (s, 6H $N(C\underline{H}_3)_2$), 3.0 (s, 1H H-2), 1.9 (s, 3H, NHAc).

2.3. Synthesis of methylated N-(4-N,N-dimethylaminocinnamyl) chitosan chloride

Previously, the methylation of chitosan and *N*-aryl chitosan derivatives has been carried out by a single treatment with

iodomethane in the presence of *N*-methyl pyrrolidone (NMP) and sodium hydroxide (Elisabete, Douglas, & Sergio, 2003; Sajomsang, Tantayanon, Tangpasuthadol, & Daly, 2008). In brief, chitosan (1.0 g) was suspended in NMP (50 mL) at room temperature for 12 h. Then 15% (w/v) of sodium hydroxide (8.0 mL) and sodium iodide (3.0 g) were added and stirred at 60 °C for 15 min. Subsequently, iodomethane (8.0 mL) was added in three portions at 3 h intervals and stirred at 60 °C for 24 h. The reaction mixture appeared as yellow and clear solution. The obtained compound was precipitated in acetone (600 mL). The precipitate was dissolved in 15% (w/v) of sodium chloride in order to replace the iodide ions with chloride ions. The suspension was dialyzed with deionized water for 3 days to remove inorganic materials and then freeze-dried to give cotton-liked powder of TMChC. Using the same technique described above, the DMCMCh was used instead of chitosan. In addition, a high degree of quaternization of TMChC was prepared by repeated methylation of TMChC as the same procedure described above.

TMChC. FT-IR; ν 3438 (O–H and N–H, GlcN), 2927, 2885, and 2849 (C–H, GlcN), 1642 (N–H, GlcNAc), 1478 (C–H, $N^+(CH_3)_3$), 1151 (C–O–C, GlcN), 1053 and 1029 cm^{-1}(C–O, GlcN). ^1H NMR (D_2O): δ (ppm) 5.4 (br. s; 1H H1′), 4.4–3.0 (br. m; 22H H2-H6, s; 6H 3, 6-*O*-$C\underline{H}_3$; s, 9H $N^+(C\underline{H}_3)_3$), 2.7 (br. m; 6H $N(C\underline{H}_3)_2$), 2.3 (s; 3H $NHC\underline{H}_3$), 1.9 (s; 3H NHAc). ^{13}C NMR (D_2O): δ (ppm) 96.5 (C1), 77.6 (C4), 74.7 (C5), 68.8 (C5), 60.0–55, (C2 and C6), 54.4 ($N^+(\underline{C}H_3)_3$), 42.7 ($N(\underline{C}H_3)_2$).

MDMCMChC. FT-IR; ν 3444 (O–H and N–H, GlcN), 3030, 2924, 2849, and 2824 (C–H, GlcN), 1654 (N–H, GlcNAc), 1508 (C=C, Aromatic), 1472 (C–H, $N^+(CH_3)_3$), 1117 (C–O–C, GlcN), 1081 and 1059 (C–O, GlcN), and 852 cm^{-1} (C–H, Aromatic). ^1H NMR (D_2O): δ (ppm) 7.9–7.3 (m, 4H, Ph), 6.7–6.3 (dd, 2H $C\underline{H}$=$C\underline{H}$), 5.3 (s, 1H H1′), 4.8–3.1 (31H, m, 7H $C\underline{H}_2$-NH and H3-H5; s, 9H $N^+(C\underline{H}_3)_3$ Ph; s, 6H 3, 6-*O*-CH_3; s, 9H $N^+(C\underline{H}_3)_3$), 3.0 (s, 1H H-2), 2.4 (s, 3H $NHC\underline{H}_3$), 1.9 (s, 3H, NHAc).

2.4. Characterization of chitosan derivatives

All Fourier transform infrared (FT-IR) spectra were collected with a Nicolet 6700 spectrometer (Thermo Company, USA) by using potassium bromide pellets at ambient temperature (25 °C). The spectra were collected using standard spectral collection techniques and the rapid-scan software in OMNIC 7.0. In all cases spectra were collected using 32 scans with a resolution of 4 cm^{-1}. The ^1H NMR spectra were measured on ADVANCE AV 500 MHz spectrometer (Bruker, Switzerland). All measurements were performed at 300 K, using pulse accumulation of 64 scans and an LB parameter of 0.30 Hz. D_2O/CD_3COOD and D_2O were used as the solvents for 5 mg of chitosan and methylated chitosan derivatives, respectively.

2.5. Molecular weight determination

The weight average molecular weight (M_w), number average molecular weight (M_n), and M_w/M_n of chitosan derivatives were determined by using the gel permeation chromatography (GPC). The M_n, M_w and M_w/M_n of the chitosan were found as 48.71 kDa, 276.06 and M_w/M_n 5.67, respectively. The GPC consists of Waters 600E Series generic pump, injector, ultrahydrogel linear columns (M_w resolving range 1–20,000 kDa), guard column, pollulans as standard (M_w 5.9–788 kDa), and refractive index detector (RI). All samples were dissolved in acetate buffer, pH 4 and then filtered through VertiPure nylon syringes filters 0.45 μm (Vertical chromatography Co., Ltd., Thailand). The mobile phases, 0.5 M AcOH and 0.5 M AcONa (acetate buffer pH 4), were used at a flow rate of 0.6 mL/min at 30 °C. Then the injection volume of 20 μL was used.

2.6. Preparation of nanocomplexes

Chitosan derivative solutions (1 mg/mL) and DS at various concentrations ranging from 0.2 to 5 mg/mL were prepared in distilled water, which was passed through 0.22 μm membrane filter. Each 1 mL of DS solution and chitosan derivative solutions was mixed and stirred at 300 rpm for 30 min to obtain nanocomplexes with weight ratio ranging from 0.2 to 5:1 (w/w).

2.7. FT-IR study of nanocomplexes

The change in functional groups of dried DS nanocomplexes at weight ratio of 2:1 (drug/polymer) were observed by FT-IR using a Nicolet 6700 spectrometer (Thermo Company, USA). All FT-IR spectra were collected by using potassium bromide pellets at ambient temperature (25 °C) and using standard spectral collection techniques and the rapid-scan software in OMNIC 7.0. In all cases spectra were collected using 32 scans with a resolution of 4 cm^{-1}.

2.8. Measurement of particle size and zeta potential of nanocomplexes

Measurement of particle size, polydispersity index (PDI) and zeta potential of the DS nanocomplexes was performed by using photon correlation spectroscopy (PCS; NanoZS4700 nanoseries, Malvern Instruments, UK). The particle size and zeta potential were reported as the average of three measurements at 25 °C.

To determine the effect of salt (NaCl) concentration on nanocomplex formation, the complex was formed at optimal weight ratio of 1.4 and 1:1 and magnetically stirred for 30 min. Specified volumes (0.5 mL) of a NaCl stock solution, prepared in DI water, were added to the complexes to obtain salt concentrations ranging from 0.1 M to 2 M, stirred for 10 min and thereafter the size analysis were determined by PCS. A separate sample for analysis was prepared for each salt concentration. For each sample, the mean of three determinations was calculated for the size analysis. Control measurements were also performed on DS solution at equal amount as in the nanocomplexes.

2.9. Particle morphology study by Atomic Force Microscope (AFM)

The morphology of the DS nanocomplexes was analyzed by using AFM (SPA400, Seiko, Japan). The DS nanocomplexes were prepared as mentioned earlier at the weight ratio of 2:1 (drug/polymer). Appropriate amounts of the DS nanocomplexes were diluted with distilled water at optimal dilution ratio and were dropped to freshly cleaved mica. After that the samples were placed in an atmosphere until completely dried. Subsequently, the samples were imaged by scanning 10 μm × 10 μm area in tapping mode using an NSG01 cantilever with 115–190 kHz resonance frequencies and a constant force, in the range of 2.5–10 N m^{-1}. All images were recorded in air at room temperature and a scan speed of 1 Hz, the phase image and topology image were used to determine the morphology and particle size of the DS nanocomplexes.

2.10. Drug entapment efficiency (%EE) study

The entrapment efficiency (%EE) was determined by indirect method. The DS nanocomplex suspensions were centrifuged at 18,000 rpm for 2.5 h at room temperature (25 °C) (KUBOTA 7780, Tokyo, Japan). The supernatant was collected to measure the amount of free DS by using UV–Visible spectrophotometer (Lamolecular dynamica 650, PerkinElmer, USA) at the wavelength of

276 nm. %EE was calculated using following equation:

$$\%EE = \frac{\text{initial drug loading (mg)} - \text{free drug (mg)}}{\text{initial drug loading (mg)}} \times 100 \quad (1)$$

2.11. In vitro drug release study

The DS nanocomplexes at weight ratio of 2:1 of drug/polymer (15 mg) were placed in dialysis membrane with M_w cut-off of 12,000–14,000 g/mol. The membrane was immersed in 200 mL of pH 7.4 PBS (1.4 M NaCl, 27 mM KCl, 65 mM Na_2HPO_4 and 15 mM KH_2 PO_4) with magnetically stirrer 300 rpm at 37 °C. The 3 mL of samples were collected at specified time and an equivalent volume of the fresh medium was added after sampling. The amount of DS released from the DS nanocomplexes and DS solution was determined using UV–vis spectrophotometer at the same wavelengths previously mentioned against the predetermined calibration curve. These data were carefully calculated to determine the accumulative amount of drug released from the samples at each specified period. The experiments were carried out in triplicate and the results were reported as average values.

2.12. Measurement of mucoadhesive properties of chitosan derivatives and nanocomplexes by surface plasmon resonance (SPR) method

The mucoadhesive properties of both chitosan derivatives and the DS nanocomplexes were determined by SPR method, which was modified from the BIACORE method (Takeuchi et al., 2005; Thongborisute & Takeuchi, 2008). CMD500 (carboxymethyldextran hydrogel) sensor chip surface was pre-activated with a mixture of 100 mM N-hydroxysuccinimide (NHS) and 400 mM 1-ethyl-3-(3-dimethylaminopropyl) carbodiimide hydrochloride (EDC). Mucin particle suspension at a concentration of 0.1% (w/v) was prepared in 10 mM acetate buffer (pH 4.5) as mentioned earlier. All immobilization were carried out at a flow rate of 50 μL/min. Firstly 22 kDa chitosan was injected at a concentration of 0.1% (w/v) across the activated surface for 10 min and baseline data was collected. The remaining reactive esters were transformed into inactive amides by injection of 1 M ethanolamine HCl, pH 8.5, at a flow rate of 50 μL/min. After collecting the equilibrium baseline data, mucin particle suspension was injected and the baseline was recorded until equilibrium. Afterwards, samples of 0.5% (w/v) of chitosan derivatives or DS nanocomplexes at optimal weight ratios was injected for 10 min, ensuring a complete equilibrium. The refractive index unit (RIU) for each sample was then recorded on the home-built SPR imaging system equipped with a 7-channel flowcell. Details of the SPR imaging apparatus, similar to the system previously reported (Shumaker-Parry, Aebersold, & Campbell, 2004), are briefly discussed here. The collimated light beam from an 880-nm light emitting diode (LED) was passed through a linear polarizer and an iris aperture and then illuminated the functionalized SPR sensor chip through a BK7 prism in a Kretschmann configuration. The SPR sensor chip was attached to the top surface of the prism using an index matching liquid. The reflected images from the SPR chip were collected by a near-infrared CCD camera at the imaging angle which was adjusted in a linear region of the SPR curve to get the highest image contrast (Shumaker-Parry et al., 2004). The selected incident angle was kept constant throughout the experiment. The relationship between the reflectivity change and the refractive index unit (RIU) was established just before the experiments using the solutions with known refractive indices. The term "reflectivity" in this study is defined as the ratio of the p-polarized light intensity to the s-polarized light intensity. Sample concentrations were carefully chosen to ensure that all succeeding SPR signals were well within a linear respond region of the instrument. The multichannel flow cell was made of polydimethylsiloxane (PDMS) using a precision aluminum molding technique. The volume of each flowcell channel was 5 μL. A multichannel peristaltic pump (IP-N8, Ismatec, Switzerland) was used to control the flow of samples across the sensor surface. Polyacrylic acid (~140 kDa) was used as positive control in this study.

$$\%RIU\ decrease = \frac{\text{RIU from mucin baseline to sample}}{\text{RIU from chitosan baseline to mucin}} \times 100 \quad (2)$$

3. Results and discussion

3.1. Synthesis and characterization of methylated N-(4-N,N-dimethylaminocinnamyl) chitosan chloride

The DMCMCh was carried out by reductive amination of the corresponding Schiff base intermediate. It was a versatile and specific method for creating a covalent bond between a substrate and the amine function of the chitosan. The degree of *N*-substitution (DS) was determined by the ^{1}H NMR spectroscopy. It was found that the DS and the yield of DMCMCh were 50% and 70%, respectively. Methylation of chitosan and DMCMCh was carried out by using iodomethane in the presence of NMP and sodium hydroxide yielded TMChC and MDMCMChC, respectively. The degree of quaterniztion (DQ) was determined by the ^{1}H NMR spectroscopy according to previously reported (Sieval et al., 1998). It was found that the DQ of TMChC and MDMCMChC was 65% ± 2, whereas the *N*,*N*-dimethylation was 24% ± 2. Moreover, 3-*O*-methylation and 6-*O*-methylation of TMChC and MDMCMChC were found to be 35% ± 2 and 15% ± 2, respectively.

The chemical structures of chitosan and its derivatives were characterized by FT-IR (Fig. 2a) and ^{1}H NMR spectroscopy (data not shown). The FT-IR spectrum of DMCMCh showed the additional absorption bands at wavenumbers of 1611, 1518 and 804 cm^{-1}. These bands were assigned to the C=C stretching and C–H deformation (out of plane) of the aromatic group, respectively. The MDMCMChC and TMChC exhibited the characteristic FT-IR spectrum at wavenumbers of 1472 cm^{-1} and 1478 cm^{-1} which were assigned to C–H symmetric bending of the methyl substituent of quaternary ammonium groups (Kim, Choi, Chun, & Choi, 1997). The ^{1}H NMR spectrum of DMCMCh exhibited the broad multiplet protons signals at δ 7.4 ppm and the singlet protons signal at δ 3.1 ppm, which were assigned to the aromatic protons and the *N*,*N*-dimethyl protons at *para*-position of aromatic group, respectively. The ^{1}H NMR spectrum of the MDMCMChC exhibited the proton signal at δ 3.5 ppm which assigned to the *N*,*N*,*N*-trimethyl protons of cinnamyl substituent. The protons signals at δ 3.2 and 2.7 were assigned to the *N*,*N*,*N*-trimethyl protons and *N*,*N*-dimethyl protons of GlcN, respectively. Furthermore, *O*-methylation was also observed at δ 3.3 and 3.4 ppm, which was assigned to 6-*O*-methylated and 3-*O*-methylated protons.

The weight average molecular weight (M_w), the number average molecular weight (M_n) and the M_w/M_n of chitosan and its methylated derivatives were determined by gel permeation chromatography (GPC). The M_n, M_w and M_w/M_n of TMChC was found as 22.88 kDa, 120.87 kDa and 5.28, respectively, whereas MDMCMChC was found as 65.25 kDa, 92.27 kDa and 1.41, respectively. It was found that the molecular weight of the chitosan derivatives decreased after methylation under basic condition. It was plausible that the sodium hydroxide degraded the polysaccharide backbone in such condition. Moreover, an oxidative degradation process and alkaline depolymerization lead to the methylation step accompanied by a significant molecular weight decrease.

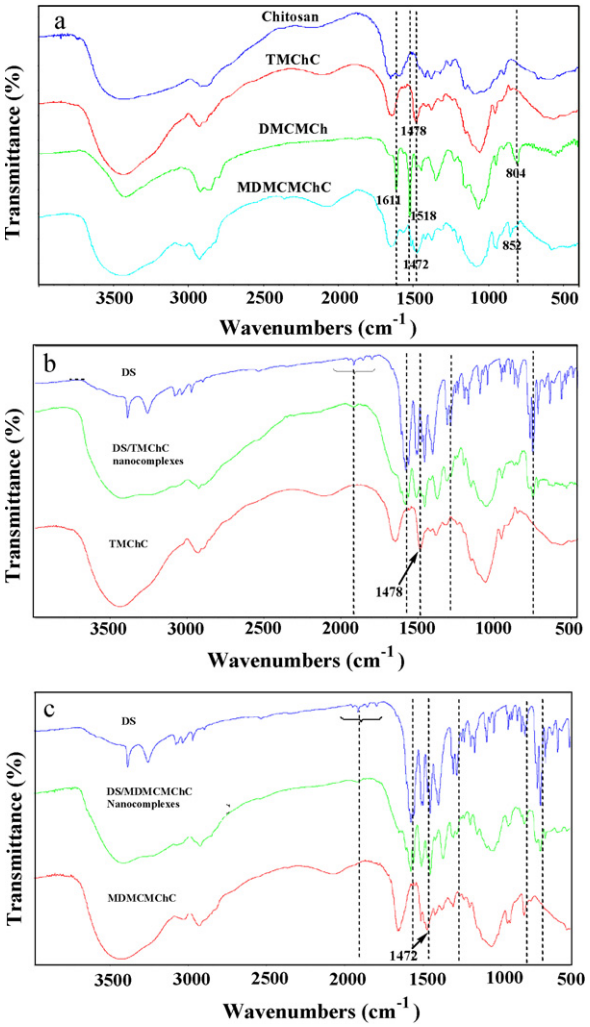

Fig. 2. FT-IR spectra of chitosan and its derivatives (a); *N*-(4-*N*,*N*-dimethylaminocinnamyl) chitosan (DMCMCh), *N*-(4-*N*,*N*,*N*-trimethylcinnamyl) chitosan chloride (DMCMChC), and *N*,*N*,*N*-trimethyl chitosan chloride (TMChC). FT-IR spectra of DS nanocomplexes; DS/TMChC (b) and DS/MDMCMChC (c) at weight ratio of 2:1. Drug (top line), DS nanocomplexes (middle line) and chitosan derivatives (bottom line).

3.2. Characterization of nanocomplexes by FT-IR

The FT-IR spectra of dried nanocomplexes at weight ratio of 2:1, DS and the chitosan derivatives are shown in Fig. 2b and c. DS showed its signature peaks at wavenumbers of 3385–3254, 3078–3036, 1944–1793, 1573 and 746 cm^{-1} which were corresponded to N–H stretching, C–H stretching, C–H out of bending overtone, C=C stretching and C–H deformation (out of plane) of the aromatic moiety, respectively. Moreover, the peaks found at 1320–1031 cm^{-1} can be assigned to C–O–C asymmetric and symmetric stretching of carboxylic group. These peaks were also observed in the DS nanocomplexes but with lower intensity when compared with the peaks of DS (Fig. 2b and c). The peaks at wavenumbers of 1478 and 1472 cm^{-1}, which were C–H symmetric bending of the methyl substituent of quaternary ammonium groups of TMChC and MDMCMChC were found on both derivatives but disappeared from the DS nanocomplexes. It was expected that the carboxylate formation in the nanocomplexes should be observed from symmetric and asymmetric carbonyl stretching, resulting in lower peak intensity. This suggested ionic interaction between the carboxylate group of DS and the quaternary ammonium group of both chitosan derivatives in the DS nanocomplexes.

3.3. Particle size and zeta potential of nanocomplexes

Ionic interaction in the nanocomplexes prepared by negatively charged DS and positiviely charged TMChC or MDMCMChC polymers was confirmed by FT-IR. The particle size and zeta potential of these nanocomplexes were measured by PCS (Fig. 3). An increase in investigated drug/polymer weight ratios from 0.2:1 to 5:1 resulted in a decrease in zeta potential of both derivatives. This implies that the negatively charged DS would interact and entrap within the chitosan chains, which is expected to project their positively charged chains toward aqueous medium. At low weight ratios of drug to polymer (0.2–0.4:1), large nanocomplexes in a range of 300–600 nm were obtained with high polydispersity index (0.65–0.85), which could be due to random deposition of DS molecules on chitosan chains. The particle size tended to decrease with an increase in weight ratios until optimal weight ratios were reached. After these optimal weight ratios, particle aggregation occurred as seen from the significantly increased particle size and the reduction in zeta potential. A minimum zeta potential of greater than 60 mV is required for an excellent stability and of greater than 30 mV for a good physical stability (Mehnert & Mader, 2001).

Stable, uniform and monodispersed DS nanocomplexes could be found at optimal weight ratio of 1.4:1 and 1.0:1 for TMChC and MDMCMChC, respectively. The obtained particle sizes at these optimal weight ratios were found at 45 ± 1 and 89 ± 5 nm with polydispersity index of 0.40 and 0.56, whereas zeta potential were 21.6 ± 2.3 and 44.1 ± 0.6 mV, respectively. It should be noted that optimal weight ratio for nanocomplex formation of MDM-

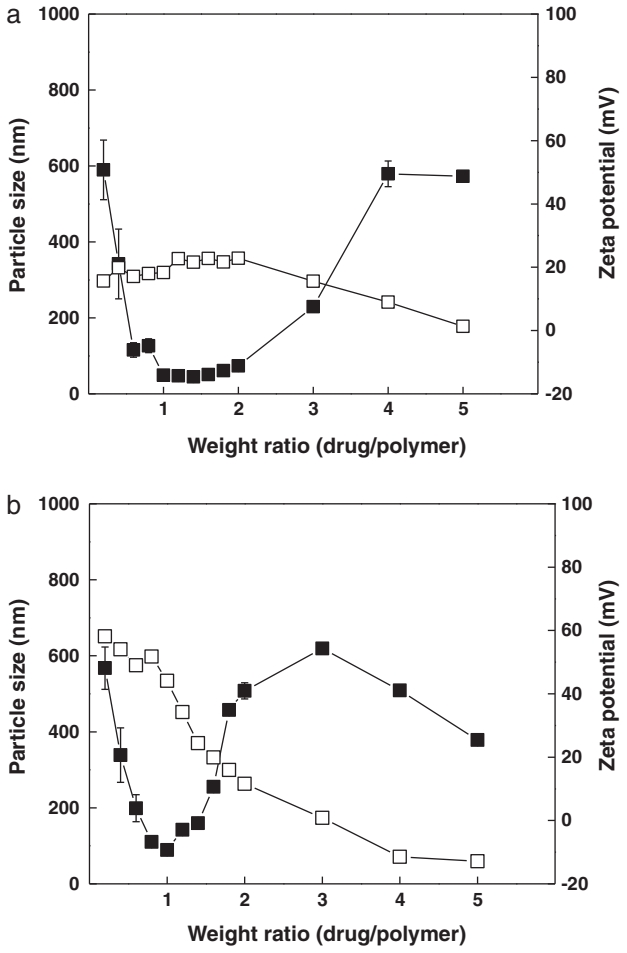

Fig. 3. The particle size (■) and zeta-potential (□) of DS/TMChC nanocomplexes (a) and DS/MDMCMChC nanocomplexes (b).

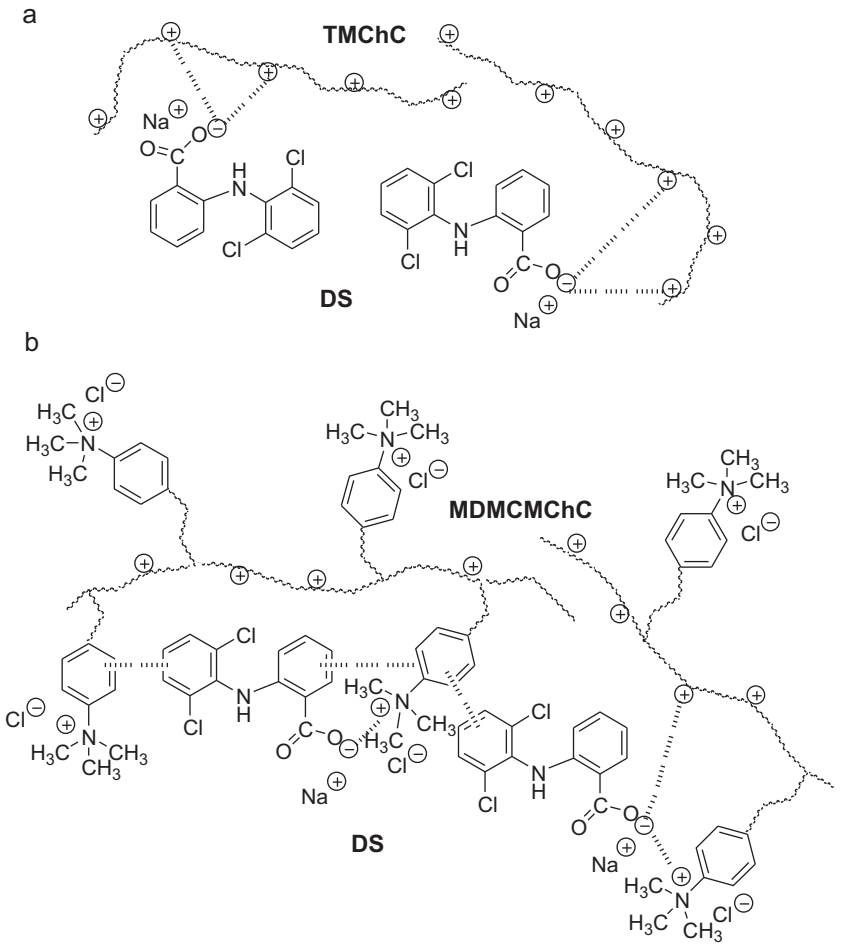

Scheme 1. Possible mechanism of drug–polymer interaction: DS/TMChC nanocomplexes (a) and DS/MDMCMChC nanocomplexes (b).

CMChC was lower as compared to TMChC. The substitution of chitosan backbone with hydrocarbon moieties of amphiphilic moieties of *N*-(4-*N*,*N*,*N*-trimethylammoniumylcinnamyl), leading to increasing hydrophobicity of MDMCMChC as compared to TMChC, plays a major role on the apparent differences. It is possible to hypothesize that complex formation between MDMCMChC and DS is initially driven by electrostatic attraction between these two ionic species and later by hydrophobic interaction between the aromatic moiety of the MDMCMChC and the aromatic ring of DS (Scheme 1). It should be noted that a presence of *N*-(4-*N*,*N*,*N*-trimethylammoniumylcinnamyl) moieties does not cause any steric hindrance on complex formation but also enhance drug association, resulting in early optimal weight ratio of MDMCMChC. Moreover, it is seen that the obtained particle size of DS/TMChC nanocomplexes were much smaller than that of DS/MDMCMChC (Fig. 3). This could be due to a presence of *N*,*N*,*N*-trimethylammonium groups of TMChC, which are readily available to interact with negatively charged carboxyl group of DS, resulting in stronger ionic interaction between two species and the formation of tightly cross-linked compact particles. In contrast, possible steric hindrance to the drug-amino group interaction as a result of an introduction of the *N*-(4-*N*,*N*,*N*-trimethylammoniumylcinnamyl) group into the chitosan backbone of MDMCMChC could occur, resulting in loose complex formation (Scheme 1). Therefore the chemical structure of chitosan derivatives has significant influence on both optimal weight ratios and the particle size of the DS nanocomplexes, which is similar to previous reports on chemical modification of chitosan to thiolated chitosan (Bravo-Osuna, Schmitz, Bernkop-Schnürch, Vauthier, & Ponchel, 2006; Sun, Mao, Mei, & Kissel, 2008), lauryl succinyl chitosan (Rekha & Sharma, 2009) and polymeric micelles (Prompruk, Govender, Zhang, Xiong, & Stolnik, 2005). It is worth noting that the size of drug-loaded nanocomplexes prepared from these new chitosan derivatives is in the sub-200 nanometer size range and may, therefore, be exploited to achieve efficient tissue penetration to target sites in the body especially for ocular delivery.

3.4. Morphology of DS nanocomplexes

AFM has been recently employed as a major microscopic tool to observe polyelectrolyte nanocomplexes size and morphology (Jintapattanakit et al., 2007; Sun et al., 2008; Yin et al., 2009). This is due to many advantages for the detection and characterization of heterogeneous populations with regards to the amount of material required for a study as well as to the level of information that can be acquired (Sriamornsak et al., 2008). Due to the soft nature of all samples, AFM with a tapping mode was used in this study to characterize its size and structure. In this mode, an oscillating probe tip taps at high frequency (ca. 300 kHz), the samples while scanning it. Advantages of this mode are that low forces and minimal damage enable it to image soft samples in air. The morphology of the DS nanocomplexes was observed with AFM at weight ratio of 2:1 of polymer/drug. Discrete particles with spherical shapes were found for both derivatives (Fig. 4). The DS nanocomplexes with uniform particle size were well dispersed with few aggregates. The images clearly indicate the presence of spherical particulates with a smooth surface and compact structure, which are similar to previous reports (Jintapattanakit et al., 2007;

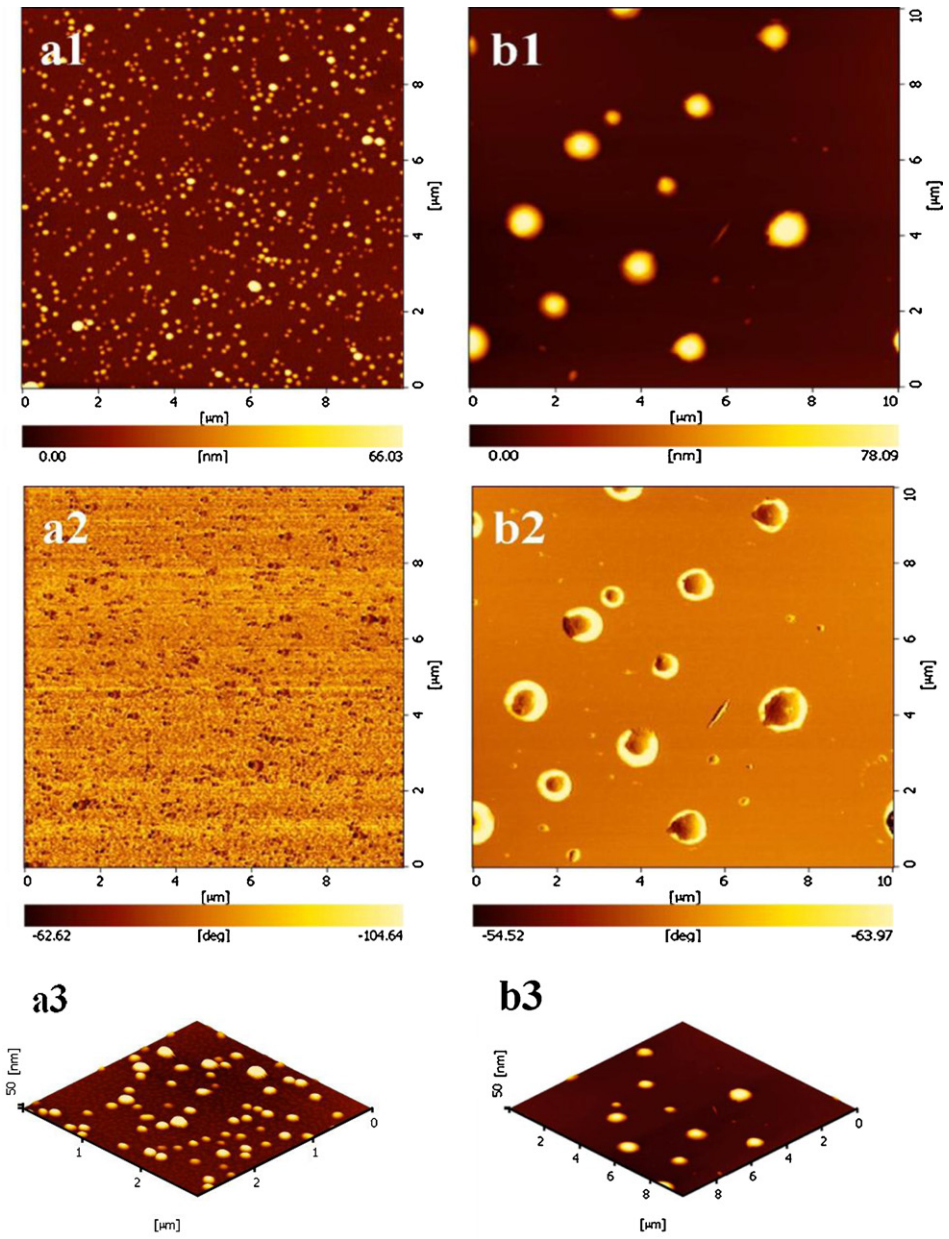

Fig. 4. Atomic force microscopy images of the DS/TMChC nanocomplexes (a) and DS/MDMCMChC nanocomplexes (b) at weight ratio of 2:1. These images reveal topology images (1), phase images (2), and 3D images (3).

Sun et al., 2008; Yin et al., 2009). The geometric mean diameter obtained from AFM is approximately 89 ± 8 nm and 490 ± 82 nm for DS/TMChC and DS/MDMCMChC nanocomplexes, respectively. Again, smaller particles were observed for the nanocomplexes formed with TMChC. Mean particles height were 28 ± 9 nm and 72 ± 12 nm for DS/TMChC and DS/MDMCMChC nanocomplexes, respectively. However, it should be noted that that even though no rigorous fixation is required for the preparation of AFM samples, the results may be influenced by lipid spreading or flattening of the complexes, which are soft and deformable, to some extent. Hence, the height of nanocomplexes measured from AFM images was less than their diameter due to the flattening of nanocomplexes while spreading onto the mica surface. AFM images demonstrated that majority of the particles were separated from one another, suggesting that these nanocomplexes were possibly stabilized against particle agglomeration, due to the ionic stabilization of positive charges at the surface of the complexes. It should be noted that in this study the size obtained from AFM were similar to the hydrodynamic diameters determined from PCS. This is in contrary to previous reports on smaller size obtained from AFM as compared to PCS (Ruozi, Tosi, Leo, & Vandelli, 2007; Sun et al., 2008). The effect has been attributed to material dehydration during sample preparation of AFM measurement whereas for PCS measurement the nanocomplexes were suspended in aqueous medium or in swelling state.

3.5. Entrapment efficiency and release characteristics of DS nanocomplexes

The incorporation of DS into chitosan derivatives and its entrapment efficiency was performed by the indirect method (Fig. 5a). The result indicated that the %EE increased with increasing weight ratio, until the maximum %EE found at optimal weight ratio of 1.4:1 and 1:1 for DS/TMChC and DS/MDMCMChC, respectively were

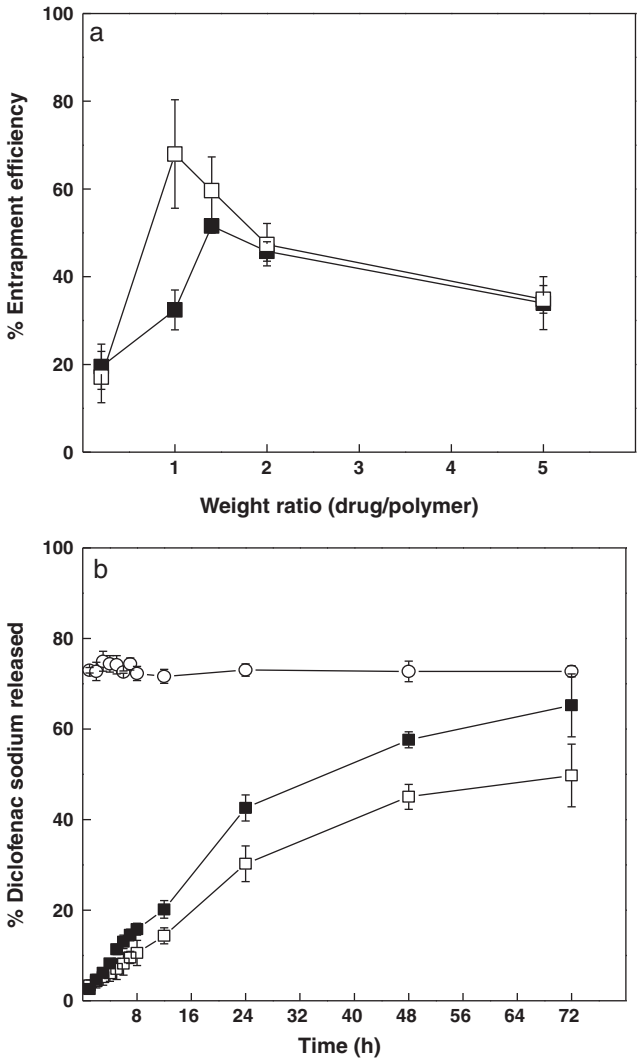

Fig. 5. % Entrapment efficiency (a) at varying weight ratio of the DS/TMChC (■), DS/MDMCMChC (□) nanocomplexes and drug release profile (b) of the nanocomplexes (■, □) compared with a control, DS solution (○).

51.6 ± 1.6 and 68.0 ± 12.4%. On the contrary, after these ratios %EE decreased with the increase of weight ratio of drug/polymer. These results agreed well with the other groups (Fredheim & Christensen, 2003; Jintapattanakit et al., 2007) who reported maximum association efficiency and process yield of lignosulfonate-chitosan, TMC400/insulin and PEG(5k)40-g-TMC100 nanocomplexes can be found at optimal charge ratio. Then both yields declined when increasing ratios of chitosan. This phenomenon in our study could be explained by when DS concentration increased, the charge density of negatively charged drug increased. This may hinder the polymer to associate with the drug molecules, causing low %EE (Prompruk et al., 2005).

It should be noted that the %EE of MDMCMChC was much higher than that of TMChC. An increased amount of drug associated with the MDMCMChC derivatives indicates an augmentative role of the *N*-(4-*N*,*N*,*N*-trimethylammoniumylcinnamyl) moieties in drug-incorporation, thereby creating a system with increased drug-entrapment efficiency. The results confirmed that the presence of hydrophobic moieties in this derivative, therefore, appears to have resulted in hydrophobic/aromatic intermolecular interactions that could lead to the observed increased molecular association. It is possible that hydrophobic interaction occurs and stabilizes the DS nanocomplexes (Scheme 1).

An *in vitro* release study was performed on the DS/TMChC and DS/MDMCMChC nanocomplexes at weight ratio of 2:1 by using dialysis membrane (Fig. 5b). The control of this study is the release of DS solution across the dialysis membrane. The release profile of the DS/MDMCMChC nanocomplexes differed significantly from that of the DS/TMChC system. The DS/TMChC system displayed a drug release of approximately 15% in the first 8 h while the DS/MDMCMChC system demonstrated a drug release of approximately 10% within the first 8 h. The DS/TMChC nanocomplexes displayed a higher drug release with approximately 65% of the drug released from the nanocomplexes within the 72 h while for the DS/MDMCMChC nanocomplexes the drug release was only 50%. The release profiles of the DS nanocomplexes were best fitted into the Higuchi model, where drug release from a matrix system is directly proportional to the square root of time. Linear fits were obtained after excluding time points after 8 h indicating that the release profile of the DS nanocomplexes occurred by diffusion mechanism. Release kinetic parameters (R^2 and k values) were obtained. The R^2 values obtained from the Higuchi model plot were 0.9904 and 0.9941 for DS/TMChC and DS/MDMCMChC nanocomplexes, respectively while the release rate (k value) were 1.98 and 1.03 $h^{-0.5}$, respectively. The calculated release rate of DS/MDMCMChC nanocomplexes is much slower than that of DS/TMChC nanocomplexes. Therefore, the DS/MDMCMChC nanocomplexes were able to show a more controlled release of DS as compared to *N*-(4-*N*,*N*,*N*-trimethylammoniumylcinnamyl) moieties-free chitosan derivative such as TMChC. These results are in closed agreement with previous report where a presence of hydrophobic (lauryl) moieties slowed down the release characteristics of the insulin at pH 1.2 compared to the native chitosan particles (Rekha & Sharma, 2009). An effect of hydrophobic N-acylated chitosan matrices for controlled drug delivery applications where the hydrophobic interactions of longer acyl chain substitution are believed to enhance the stability of substituted chitosan, resulting in prolonged release of the drug has also been reported (Tein, Lacroix, Ispas-Szabo, & Mateescu, 2003).

3.6. Effect of salt (NaCl) concentration on complex formation

It is known that the stability of polyionic complexes is strongly influenced by the ionic strength of the medium: being destabilised with an increase in ionic strength due to electrostatic shielding (Govender et al., 2001; Harada & Kataoka, 1997). The influence of salt concentration on complex formation between DS and both chitosan derivatives (MDMCMChC and TMChC) was therefore determined by measuring the size of the nanocomplexes after the addition of NaCl at various concentrations (Fig. 6). The effect of salt on DS solution in the same concentration was also undertaken as a control (Fig. 6c). The results clearly demonstrate that the size of DS nanocomplexes, was influenced by the salt concentration. As the NaCl concentration was increased from 0.1 M to 1.5 M, particle size also increased from nanometer range to micrometer range. An increase in salt concentration may possibly have induced complex aggregation and dissociation of the complexes afterwards, due to electrostatic shielding. It is seen that with the addition of salt DS may dissociate from the nanocomplexes to be free DS in solution. Since DS had low water solubility in the sodium-rich medium, this would lead to the precipitation of DS as seen in control experiment due to the common ion effect (Fig. 6c). More pronounced effect was found for DS/TMChC (Fig. 6a) as compared to DS/MDMCMChC nanocomplexes (Fig. 6b), suggesting that DS/TMChC nanocomplexes is much more salt-sensitive. Therefore, the salt effect study indicates that electrostatic interaction plays an important role on complex formation of TMChC with DS than MDMCMChC. Major role of non-electrostatic interactions particularly hydrogen bonding which was dominant in stabilising the complex between cationic

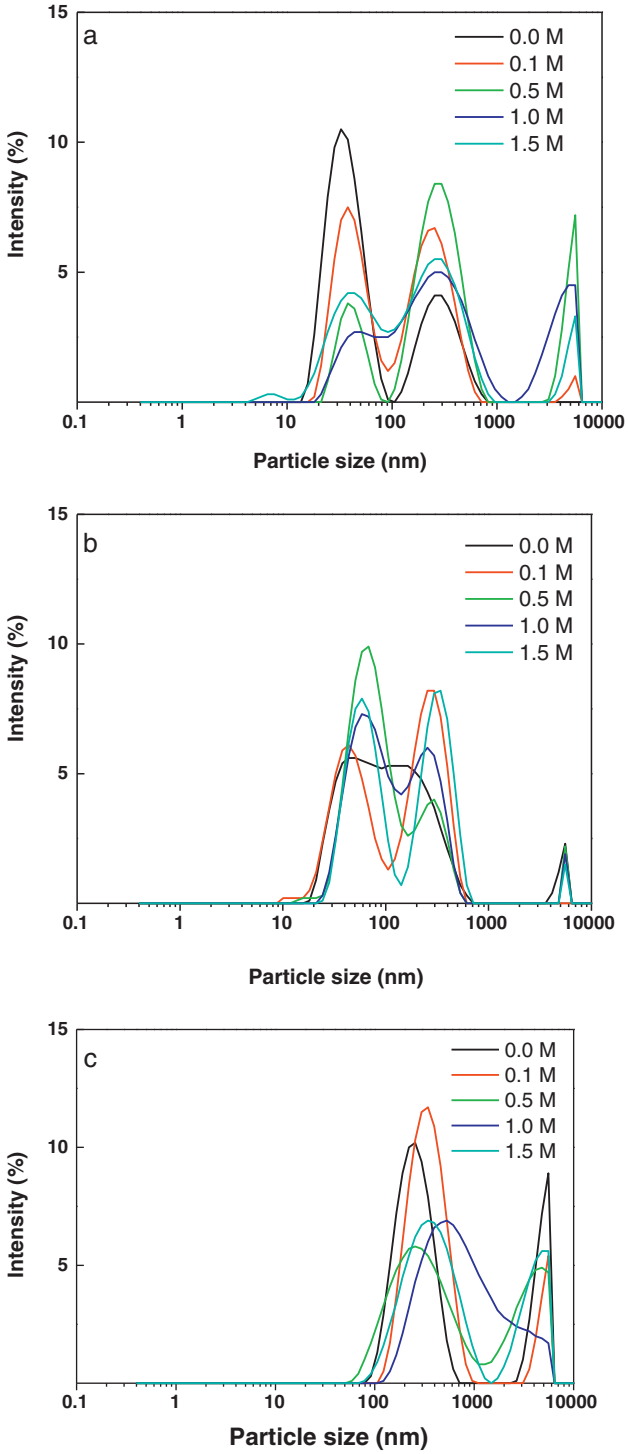

Fig. 6. Effect of salt (NaCl) concentration on DS/TMChC (a) and DS/MDMCMChC (b) nanocomplexes compared with a control, DS solution (c).

diminazene aceturate with anionic poly(aspartic acid) and procaine hydrochloride with polyacrylic acid have been reported (Ehtezazi, Govender, & Stolnik, 2000; Govender, Ehtezazi, Stolnik, Illum, & Davis, 1999). The interactions between these molecules have been studied at varying salt concentration by using isothermal titration microcalorimetry. Clearly, future studies to determine the type of dominant force and thermodynamic parameters of the interaction between DS and these two derivatives will be necessary to assess the nature of the *N*-(4-*N*,*N*,*N*-trimethylammoniumylcinnamyl) role in drug association.

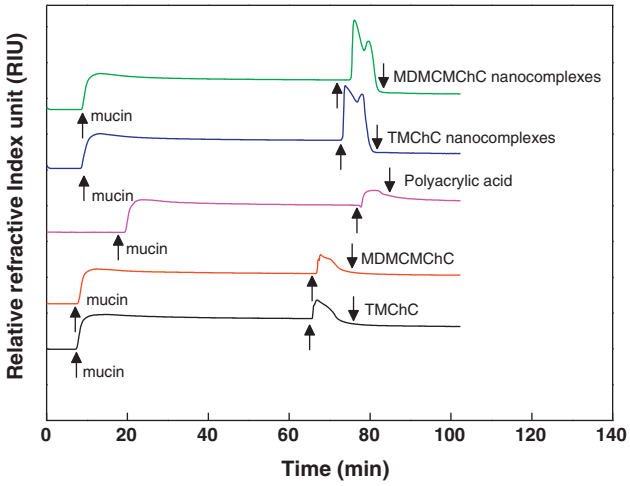

Fig. 7. Overlay sensograms for mucin-immobilized CMD500 sensor chip after injection of 0.5% (w/w) chitosan derivatives (TMChC and MDMCMChC), polyacrylic acid and their DS nanocomplexes at optimal weight ratio. ↑ mucin ↓ mucin: start and stop mucin injection; ↑ sample ↓ sample: start and stop sample injection.

3.7. Mucoadhesive properties of chitosan derivatives and their DS nanocomplexes by surface plasmon resonance (SPR) method

In our study, a commercial lyophilised porcine ss-mucin (type III) was often used due to its less batch-to-batch variability and high reproducibility for mucoadhesive test (Rossi, Ferrari, Bonferoni, & Caramella, 2000, 2001). According to the principle of the BIACORE method using SPR (Takeuchi et al., 2005), if the binding between mucin and the polymers occurs, the response on a prepared sensor surface will increase as the sample pass over it. If equilibrium is reached, a constant signal will be seen. Therefore the strength of binding can be determined from the change of refractive index unit (RIU) response (Thongborisute & Takeuchi, 2008). Fig. 7 shows the mucoadhesion of both chitosan derivatives and their DS nanocomplexes to mucin. The RIU response increased after mucin injection to immobilized sensor chip surface. An increase in RIU response was due to the change of refractive index on the sensor chip surface when there is a binding between injected molecules (mucin) and immobilized molecules (chitosan). The RIU responses of chitosan derivatives and their DS nanocomplexes decreased, when all samples were passed over the mucin-immobilized sensor chip surface. This could be explained by the ability of chitosan derivatives and their DS nanocomplexes to hold mucin particles on the sensor chip surface, leading to dissociation of the mucin from the sensor surface (Thongborisute & Takeuchi, 2008). The response changes after the injection of chitosan derivatives and their DS nanocomplexes were calculated as %RIU decreased. The values of decreases in RIU response of TMChC and MDMCMChC were $25.6 \pm 4.7\%$ and $8.5 \pm 2.0\%$, respectively. TMChC demonstrated much larger decreases in RIU response than MDMCMChC and relatively similar to polyacrylic acid ($27.7 \pm 0.7\%$). These SPR results correspond well with the result obtained from the mucin particle method, which has been previously reported by our group (Sajomsang, Ruktanonchai, et al., 2009). The mucin method is based on the changes in particle size and surface charges of commercially available porcine mucin particle upon the adhesion of various amounts of polymers. It was expected that the strong mucoadhesive property of the polymer would result in aggregation between polymer and mucin particles when the two species were mixed (Takeuchi et al., 2005; Thongborisute & Takeuchi, 2008). The critical concentrations of chitosan derivatives (%w/v), calculated when zeta potential equal to zero, were found at 0.24 and 0.48% (w/v), respectively for TMChC and MDM-

CMChC (data not shown), suggesting stronger affinity of TMChC towards mucin than that of MDMCMChC. A possible explanation for greater mucoahesive property of TMChC could be due to shorter and more flexible side chain of TMChC than MDMCMChC, resulting in better interpenetration of TMChC towards mucin (Andrews, Laverty, & Jones, 2009). The steric hindrance of *N*-(4-*N*,*N*,*N*-trimethylammoniumylcinnamyl) group of MDMCMChC would occur and that may shield positively charged groups of the *N*,*N*,*N*-trimethylammonium groups on the GlcN of chitosan (Sajomsang, Gonil, et al., 2009).

However, once nanocomplexes of both derivatives were formed with DS, the significant increases in RIU response were found at $48.7 \pm 2.8\%$ and $44.8 \pm 4.1\%$ for DS/TMChC and DS/MDMCMChC nanocomplexes, respectively. Thus, these results demonstrated that both DS nanocomplexes could bind stronger to mucin particle than its derivatives. This result could be due to small size in nanometer range, increased surface area and positively charged zeta potential of nanocomplexes as compared to chitosan derivatives. It should also be noted that in this study, apart from electrostatic interaction between primary amino group of cationic mucoadhesive polymers and the negatively charged sialic acid and sulphonic acid residues of mucus or mucin particles, other forces such as hydrogen bonding (the hydroxyl and amino groups of chitosan may interact with mucus via hydrogen bonding) and hydrohobic forces bound to the mucin particles may occur and govern the interaction between these DS nanocomplexes and mucin particles (Takeuchi et al., 2005).

4. Conclusions

Self-assembled nanocomplexes between water-soluble chitosan derivatives, MDMCMChC, and negatively charged DS were successfully formed. It indicates that the introduction of a relatively more hydrophobic group of *N*-(4-*N*,*N*,*N*-trimethylammoniumylcinnamyl) moiety to chitosan backbone would provide better incorporation of DS into the nanocomplexes by hydrophobic interaction, while the presence of a quaternary ammonium group would initiate electrostatic interactions with carboxylate group of DS. The chemical modification of chitosan and drug/polymer weight ratios majorly influenced physicochemical characteristics of the DS nanocomplexes, but not on its mucoadhesiveness as confirmed by SPR method. The DS nanocomplexes had a small particle size in nanometer range of 40–90 nm, appropriate for drug-targeting purposes. AFM studies confirmed the presence of these constructs as being discrete particles with fairly uniform in size and spherical shape. The presence of hydrophobic moiety, *N*-(4-*N*,*N*,*N*-trimethylammoniumylcinnamyl) substitution, with similar degree of quaternization could contribute not only to enhanced binding affinity resulting in higher drug entrapment, but also slower drug-release profile relative to TMChC. According to salt effect study, it can therefore be concluded that apart from electrostatic interaction, which are essential to initiate interaction between negatively charged drug and positively charged chitosan, the non-electrostatic interactions, such as hydrophobic interaction may dominate and stabilize the nanocomplex. This study hence demonstrated that MDMCMChC was promising chitosan derivative that can be used as mucoadhesive polymeric platform for drug delivery.

Acknowledgements

This research was financially supported by National Nanotechnology Center (NANOTEC), Thailand (Research grant number NN-B-22-EN4-94-51-10 and NN-B-22-EN7-94-51-20). The authors are grateful for Ms. Jutamas Pontrakoon for laboratory assistance.

References

Andrews, G. P., Laverty, T. P., & Jones, D. S. (2009). Mucoadhesive polymeric platforms for controlled drug delivery. *European Journal of Pharmaceutics and Biopharmaceutics*, *71*, 505–518.

Bravo-Osuna, I., Schmitz, T., Bernkop-Schnürch, A., Vauthier, C., & Ponchel, G. (2006). *International Journal of Pharmaceutics*, *316*, 170–175.

Chen, F., Zhang, Z. R., Yuan, F., Qin, X., Wang, M., & Huang, Y. (2008). *In vitro* and *in vivo* study of *N*-trimethyl chitosan nanoparticles for oral protein delivery. *International Journal of Pharmaceutics*, *349*, 226–233.

Domard, A., Rinaudo, M., & Terrassin, C. (1986). New method for the quaternization of chitosan. *International Journal of Biological Macromolecules*, *8*, 105–107.

Domard, A., Gey, C., Rinaudo, M., & Terrassin, C. (1987). ^{13}C and ^{1}H NMR spectroscopy of chitosan and *N*-trimethyl chloride derivatives. *International Journal of Biological Macromolecules*, *9*, 233–327.

Ehtezazi, T., Govender, T., & Stolnik, S. (2000). Hydrogen bonding and electrostatic interaction contributions to the interaction of a cationic drug with polyaspartic acid. *Pharmaceutical Research*, *17*, 871–878.

Elisabete, C., Douglas, D. B., & Sergio, P. C. F. (2003). Methylation of chitosan with iodomethane: Effect of reaction conditions on chemoselectivity and degree of substitution. *Macromolecular Bioscience*, *3*, 571–576.

Fredheim, G. E., & Christensen, B. E. (2003). Polyelectrolyte complexes: Interactions between lignosulfonate and chitosan. *Biomacromolecules*, *4*, 232–239.

Govender, T., Ehtezazi, T., Stolnik, S., Illum, L., & Davis, S. S. (1999). Complex formation between the anionic polymer (PAA) and a cationic drug (procaine HCl): Characterization by microcalorimetric studies. *Pharmaceutical Research*, *16*, 1125–1131.

Govender, T., Stolnik, S., Xiong, C., Zhang, S., Illum, L., & Davis, S. S. (2001). Drug–polyionic block copolymer interactions for micelle formation: Physicochemical characterization. *Journal of Controlled Release*, *75*, 249–258.

Harada, A., & Kataoka, K. (1997). Formation of stable and monodispersive polyion complex micelles in aqueous medium from poly(L-lysine) and poly(ethylene glycol)–poly(aspartic acid) block copolymer. *Pure and Applied Chemistry*, *A34*, 2119–2133.

He, W., Guo, X., & Zhang, M. (2008). Transdermal permeation enhancement of *N*-trimethyl chitosan for testosterone. *International Journal of Pharmaceutics*, *356*, 82–87.

Illum, L. (1998). Chitosan and its use as a pharmaceutical excipient. *Pharmaceutical Research*, *15*, 1326–1331.

Jia, Z., Shen, D., & Xu, W. (2001). Synthesis and antibacterial activities of quaternary ammonium salt of chitosan. *Carbohydrate Research*, *333*, 1–6.

Jintapattanakit, A., Junyaprasert, V. B., Mao, S., Sitterberg, J., Bakowsky, U., & Kissel, T. (2007). Peroral delivery of insulin using chitosan derivatives: A comparative study of polyelectrolyte nanocomplexes and nanoparticles. *International Journal of Pharmaceutics*, *342*, 240–249.

Jintapattanakit, A., Mao, S., Kissel, T., & Junyaprasert, V. B. (2008). Physicochemical properties and biocompatibility of N-trimethyl chitosan: Effect of quaternization and dimethylation. *European Journal of Pharmaceutics and Biopharmaceutics*, *70*, 563–571.

Kim, C. H., Choi, J. W., Chun, H. J., & Choi, K. S. (1997). Synthesis of chitosan derivatives with quaternary ammonium salt and their antibacterial activity. *Polymer Bulletin*, *38*, 387–393.

Mehnert, W., & Mader, K. (2001). Solid lipid nanoparticles: Production, characterization and applications. *Advanced Drug Delivery Reviews*, *47*, 165–196.

Muzzarelli, R. A. A., & Tanfani, F. (1985). The N-permethylation of chitosan and the preparation of N-trimethyl chitosan iodide. *Carbohydrate Polymers*, *5*, 297–307.

Nagarwal, R. C., Kant, S., Singh, P. N., Maiti, P., & Pandit, J. K. (2009). Polymeric nanoparticulate system: A potential approach for ocular drug delivery. *Journal of Controlled Release*, *136*, 2–13.

Prabaharan, M., & Mano, J. F. (2005). Chitosan-based particles as controlled drug delivery systems. *Drug Delivery*, *12*, 41–57.

Prompruk, K., Govender, T., Zhang, S., Xiong, C. D., & Stolnik, S. (2005). Synthesis of a novel PEG-*block*-poly(aspartic acid-*stat*-phenylalanine) copolymer shows potential for formation of a micellar drug carrier. *International Journal of Pharmaceutics*, *297*, 242–253.

Rekha, M. R., & Sharma, C. P. (2009). Synthesis and evaluation of lauryl succinyl chitosan particles towards oral insulin delivery and absorption. *Journal of Controlled Release*, *135*, 144–151.

Rossi, S., Ferrari, F., Bonferoni, M. C., & Caramella, C. (2000). Characterization of chitosan hydrochloride-mucin interaction by means of viscosimetric and turbidimetric measurements. *European Journal of Pharmaceutical Sciences*, *10*, 251–257.

Rossi, S., Ferrari, F., Bonferoni, M. C., & Caramella, C. (2001). Characterization of chitosan hydrochloride-mucin rheological interaction: Influence of polymer concentration and polymer:mucin weight ratio. *European Journal of Pharmaceutical Sciences*, *12*, 479–485.

Rúnarsson, Ö. V., Holappa, J., Nevalainen, T., Hjálmarsdóttir, M., Järvinen, T., Loftsson, T., et al. (2007). Antibacterial activity of methylated chitosan and chitooligomer derivatives: Synthesis and structure activity relationships. *European Polymer Journal*, *43*, 2660–2671.

Ruozi, B., Tosi, G., Leo, E., & Vandelli, M. A. (2007). Application of atomic force microscopy to characterize liposomes as drug and gene carriers. *Talanta*, *73*, 12–22.

Sajomsang, W., Tantayanon, S., Tangpasuthadol, V., & Daly, W. H. (2008). Synthesis of methylated chitosan containing aromatic moieties: Chemoselectivity and effect on molecular weight. *Carbohydrate Polymers*, *72*, 740–750.

Sajomsang, W., Gonil, P., & Saesoo, S. (2009). Synthesis and antibacterial activity of methylated N-(4-N,N-dimethylaminocinnamyl) chitosan chloride. *European Polymer Journal*, *45*, 2319–2328.

Sajomsang, W., Ruktanonchai, R. U., Gonil, P., & Nuchuchua, O. (2009). *Carbohydrate Polymers*, *78*, 945–952.

Sandri, G., Rossi, S., Bonferoni, M. C., Ferrari, F., Zambito, Y., Colo, G. D., et al. (2005). Buccal penetration enhancement properties of *N*-trimethyl chitosan: Influence of quaternization degree on absorption of a high molecular weight molecule. *International Journal of Pharmaceutics*, *297*, 146–155.

Shumaker-Parry, J. S., Aebersold, R., & Campbell, C. T. (2004). Parallel, quantitative measurement of protein binding to a 120-element double-stranded DNA array in real time using surface plasmon resonance microscopy. *Analytical Chemistry*, *76*, 2071–2082.

Sieval, A. B., Thanou, M., Kotzé, A. F., Verhoef, J. C., Brussee, J., & Junginger, H. E. (1998). Preparation and NMR characterization of highly substituted N-trimethyl chitosan chloride. *Carbohydrate Polymers*, *36*, 157–165.

Sriamornsak, P., Thirawong, N., Nunthanid, J., Puttipipatkhachorn, S., Thongborisute, J., & Takeuchi, H. (2008). *Carbohydrate Polymers*, *71*, 324–329.

Sun, W., Mao, S., Mei, D., & Kissel, T. (2008). Self-assemble polyelectrolyte nanocomplexes between chitosan derivatives and enoxaparin. *European Journal of Pharmaceutics and Biopharmaceutics*, *69*, 417–425.

Takeuchi, H., Thongborisute, J., Matsui, Y., Sugihara, H., Yamamoto, H., & Kawashima, Y. (2005). Novel mucoadhesion tests for polymers and polymer-coated particles to design optimal mucoadhesive drug delivery systems. *Advanced Drug Delivery Reviews*, *57*, 1583–1594.

Tein, C. L., Lacroix, M., Ispas-Szabo, P., & Mateescu, M. A. J. (2003). N-acylated chitosan: Hydrophobic matrices for controlled drug release. *Journal of Controlled Release*, *93*, 1–13.

Thongborisute, J., & Takeuchi, H. (2008). Evaluation of mucoadhesiveness of polymers by BIACORE method and mucin-particle method. *International Journal of Pharmaceutics*, *354*, 204–209.

Van der Lubben, I. M., Verhoef, J. C., Borchard, G., & Junginger, H. E. (2001). Chitosan and its derivatives in mucosal drug and vaccine delivery. *European Polymer Journal*, *14*, 201–207.

Van der Merwe, S. M., Verhoef, J. C., Verheijden, J. H. M., Kotzé, A. F., & Junginger, H. E. (2004). Trimethylated chitosan as polymeric absorption enhancer for improved peroral delivery of peptide drugs. *European Journal of Pharmaceutics and Biopharmaceutics*, *58*, 225–235.

Yin, L., Ding, J., He, C., Cui, L., Tang, C., & Yin, C. (2009). Drug permeability and mucoadhesion properties of thiolated trimethyl chitosan nanoparticles in oral insulin delivery. *Biomaterials*, *30*, 5691–5700.